Journal of Ocean, Mechanical and Aerospace
-Science and Engineering-, Vol.4

February 20, 2014

Numerical Simulation of Underwater Propeller Noise

Bagheri M.R,[a*], Seif M.S,[a] and Mehdigholi H,[a]

[a)] *Sharif University of Technology, Center of Excellence in Hydrodynamic and Dynamic of Marine Vehicles, Tehran, Iran*

*Corresponding author: mrbagheri@mech.sharif.ir, mrb.bagheri@gmail.com

Paper History

Received: 23-December-2013
Received in revised form: 30-December-2013
Accepted: 10-January-2014

ABSTRACT

Noise reduction and control is an important problem in the performance of underwater acoustic systems and in the habitability of the passenger ship for crew and passenger. Furthermore, sound generated by a propeller is critical in underwater detection and it is often related to the survivability of the vessel. This paper presents a numerical study on noises of the underwater propeller for different performance conditions. The non-cavitating and blade sheet cavitation noise generated by an underwater propeller is analyzed numerically in this study. The flow field is analyzed with finite volume method (FVM), and then the time-dependent flow field data are used as the input for Ffowcs Williams–Hawkings (FW-H) formulation to predict the far-field acoustics. Noise characteristics are presented according to noise sources and conditions. The developed flow solver is applied to the model propeller in uniform inflow. Computed results are shown to be in good agreement with other numerical results. The overall results suggest that the present approach is a practicable tool for predicting cavitation and non-cavitation noise of propellers in far field.

KEY WORDS: *Propeller Noise; FVM; FW-H; Far Field.*

NOMENCLATURE

u_i	Fluid velocity component in the xi direction
u_n	Fluid velocity component normal to the surface f=0
v_i	Surface velocity components in the xi direction
v_n	Surface velocity component normal to the surface
$\delta(f)$	Dirac delta function
$H(f)$	Heaviside function
p_∞	Upstream flow pressure
p_v	Vapor pressure
ρ_l	Fluid density
U_∞	Upstream flow velocity
σ	Cavitation number.

1.0 INTRODUCTION

Acoustics design has been considered as an important character of a modern naval ship by many countries. Rapid development of sonar technology, one of the main approaches for detecting warship, has also made it more important to improve the acoustic characteristics of a modern ship. Sound generated by a propeller is critical in underwater detection, and it is often related to the survivability of the vessels. The propeller generally operates in a non-uniform wake field behind the vessel. As the propeller rotates, it is subjected to unsteady force, which leads to discrete tonal noise, and cavitation. Therefore, underwater propeller noise can be classified into cavitating and non-cavitating noise. Cavitation of the underwater propeller is the most prevalent source of underwater sound in the ocean and it is often the dominant noise source of a marine vehicle. In the past, the propeller design philosophy has been avoiding cavitation for the widest possible range of operating conditions. However, the recent demands for high vehicle speed and high propeller load have made this designing philosophy practically impossible to achieve. Therefore, underwater propeller cavitation has been more and more common in recent ocean vehicle application[1]. So both cavitating and non-cavitating noise are also important. The approach for the investigation of the underwater propeller noise is a potential-based panel method coupled with acoustic analogy. Among the various types of cavitation noise, unsteady sheet cavitation on the suction surface is known to produce the highest noise level[2]. Propeller produces pressure waves through four mechanisms [2]:

1. Displacement of water by the rotating blades of the propeller.
2. The pressure difference between the suction and pressure

surfaces of the propeller.
3. The volume fluctuations occurring on the blades that are induced by pressure drop in front and behind of the propeller (there are sheet cavitation on the blades).
4. The process of growth and collapse of sheet and cloud cavitation.

The first two causes occur for cavitating and non-cavitating states, but they are non-cavitating effects only. The latter two occur only when the propeller is experiencing cavitation [2].
Since the cavitation noise is the major source of noise of the propeller it should be analyzed accurately. The general noise spectrum of a cavitating propeller is depicted in Figure 1. The frequency range of sheet cavitation is from 10 Hz to more than 10 kHz. The low frequency noise that form the regions I and II in Figure1 is a result of sheet cavitation and appears as large bubbles on the surfaces of the blades [3].

Sharma et al. [4] have studied some marine propellers in cavitation tunnel. In their study, the difference of Sound Pressure levels (SPLs) in two states of cavitating and non-cavitating conditions is in the range of 10 to 30 dB. In this paper, the amplitude difference in the SPLs, before and after the development of cavitation in a specified center frequency, is approximately in the range of 10 to 30 dB.

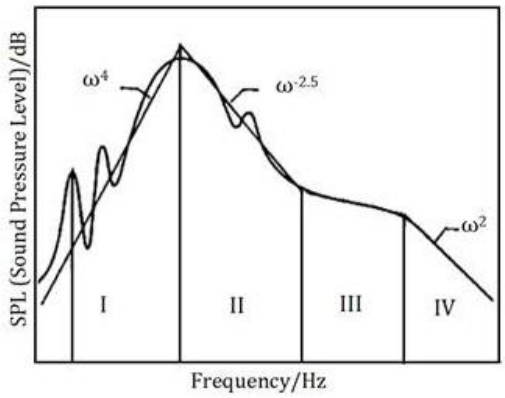

Figure 1: The frequency range of cavitation noise for marine propellers [3].

Jin-Ming et al. in 2012 investigated the noise of a three-blade propeller and concluded that the overall spectrum amplitude of sound in front of the propeller hub exceeds the propeller rotating plane [5]. Bagheri et al. in 2012 and 2013 investigated the non-cavitating/cavitating noise and hydrodynamics of marine propellers using FVM [6-8]. In this work, we used the same modeling approach, turbulence model and numerical solution method [6-8].

This paper presents a numerical study on noises of the underwater propeller for different performance conditions. The non-cavitating and blade sheet cavitation noise generated by an underwater propeller is analyzed numerically in this study. The noise is predicted using time-domain acoustic analogy. Hanshin Seol and eat al. presents a numerical study on the non-cavitating and blade sheet cavitation noises of the underwater propeller [3]. A brief summary of numerical method with verification and results are presented. The noise is predicted using FW-H formulations.

The marine propeller in its non-cavitating statue, in keeping with other forms of turbo-machinery, produces a noise signature of the type sketched in Figure 2. It is seen from this figure that there are distinct tones associated with the blade frequencies together with a broad-band noise at higher frequencies. The broadband noise comprises components derived from inflow turbulence into the propeller and various edge effects such as vortex shedding and trailing edge noise [2].

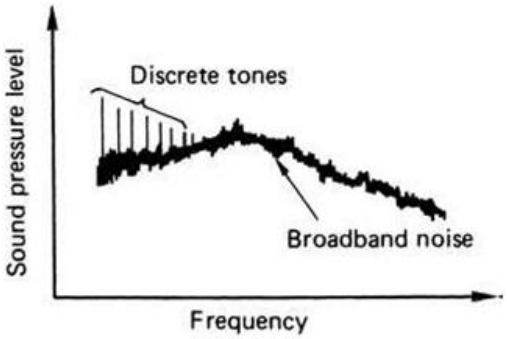

Figure2: Idealized non-cavitating noise spectrum [2].

There are various ways to evaluate Ffowcs Williams–Hawkings equation and the three types of noise source terms (monopole, dipole, and quadrupole) proposed [3]. Farassat proposed a time-domain formulation that can predict noise from an arbitrary shaped object in motion without the numerical differentiation of the observer time [9]. The implementation of this formulation is quite straightforward because contributions from each panel with different retarded times are added to form an acoustic wave. The quadruple noise source term is neglected in this study since the rotating speed of the propeller is much lower than the speed of sound in water. Through these studies, the dominant noise source of underwater propeller is analyzed. Arazgaldi and et al. present RANS simulations of flow around two different conventional propellers were carried out at non-cavitating and cavitating operating conditions using the multiphase flow model based on the “full cavitation model” proposed by Singhal et al [10]. In present paper the flow field is analyzed with finite volume method (FVM), and then the time-dependent flow field data are used as the input for Ffowcs Williams–Hawkings formulation to predict the far-field acoustics. Noise characteristics are presented according to noise sources and conditions. The developed flow solver is applied to the model propeller in uniform inflow.

2.0 METHODOLOGY

2.1 Numerical simulation

In this paper, one type propeller model of Gown series was used for investigations. The geometries and surface grids on the blade and hub surface of the propeller model are shown in Figure 3 and Table 1, respectively.

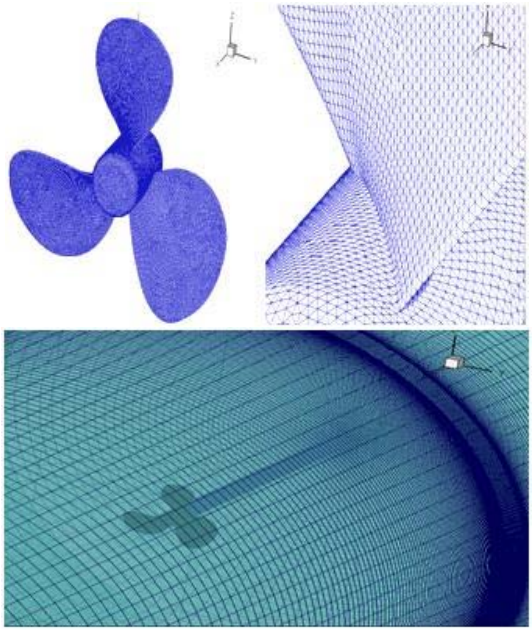

Fiugure3: Propeller 3D model and mesh grids.

Table 1: Principal particulars of propeller model.

Diameter (m)	0.3m
EAR= A_E/A_0	0.5
N. of Blade	3
Hub ratio	0.2
Series	Gown

Computational methods for cavitation flows can be largely categorized into two groups: single-phase modeling with cavitation interface tracking and multi-phase modeling with an embedded cavitation interface. The former approach has been widely adopted for inviscid flow solution methods and Euler equation solvers. In this paper is used of multi-phase model.

The cavitation model employed in the present study was introduced by Singhal et al. [12]. This model is based on multiphase flows and has the capability of accounting for the effects of slip velocity between liquid and gaseous phases. The main part of every cavitation physical model is to find the mass transfer equation between the liquid and vapor phases. In the present study, we used the following equation [12]:

$$\frac{\partial(\alpha_l\rho_l)}{\partial x} + \nabla\cdot(\alpha_l\rho_l C_m) = \Gamma_n = \dot{m}_l^v + \dot{m}_c^v \qquad (1)$$

In solving equation (1), α_l, ρ_l are the volume fraction and the density of liquid, respectively. $\dot{m}_l^v$, $\dot{m}_l^c$ are to be related to the bubble dynamics and vapor volume fraction that they defined the source terms for transfer equation. To account for the bubble dynamics, the reduced Rayleigh-Plesset equation is employed for source terms in transfer equation. The expression for $\dot{m}_l^v$, $\dot{m}_l^c$ are obtained as:

$$\dot{m}_l^v = -F^v \frac{3\rho_v\alpha_{nuc}\alpha_l}{R_0}\sqrt{\frac{2}{3}Max\left(\frac{P_v-P}{\rho_l},0\right)} \qquad (2)$$

$$\dot{m}_c^v = -F^c \frac{3\rho_v(1-\alpha_l)}{R_0}\sqrt{\frac{2}{3}Max\left(\frac{P_v-P}{\rho_l},0\right)} \qquad (3)$$

In equations (2) and (3) F^v *and* F^c are two empirical constants and Singhal et al. [12] used 0.01 and 50 for F^v *and* F^c, respectively. α_{nuc} is the volume fraction of non-condensing gases, ρ_v is the density of water vapor, p_v is the saturate pressure of water vapor and p is the flow pressure.

The main parts of the numerical simulation of any geometry are kind, size and the meshing quality, such that their compositions severely convergence / divergence and the convergent time of the problem under consideration. First, the blade surface is meshed with triangles [6-8]. The region around the root, tip and blade edges is meshed with smaller triangles, i.e. with sides of approximately 0.005 D. The inner region is filled with triangles of approximately increased size and with aspect ratios of 1.05 and 1.1. In order to resolve the boundary layer on the solid surfaces, four layers of prismatic cells with a stretching ratio of 1.1 are grown from the blade and hub surfaces.

Finally, the remaining region in the domain is filled with tetrahedral cells. Flow domain around propeller and hub set is divided two parts, first part is called moving zone and second part is called stationary zone. The propeller computational domain is cylindrical shape surrounding the propeller where a rotational cylinder with sufficient larger diameter than the propeller diameter enfolds the propeller in its cross section center and allows the fluid to pass by the model. The rotating zone was solved via Moving Reference Frame (MRF) [6-8].

The inlet is 4D upstream; the outlet is 10D downstream; solid surfaces on the blades and hub are centered at the coordinate system origin and aligned with uniform inflow; and the outer boundary is 5D from the hub axis [6-8]. The computational domain for propeller model is shown in Figure 4.

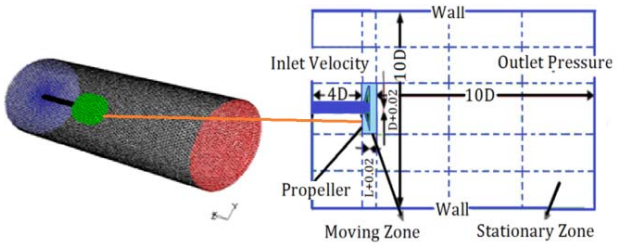

Figure 4: Computational domain around propeller (moving zone and stationary zone) and boundary conditions.

In order to simulate the flow around a rotating propeller, the boundary conditions are as flowing:
On the inlet boundary, velocity components are imposed for a uniform stream with a given inflow speed; on the blade and hub surface, a no slip condition is imposed; on the lateral boundary, a slip boundary condition is imposed; and on the outlet boundary, the pressure is set to a constant value[6-8].

Table 2: Different parameters of flow and acoustic conditions.

statue	Va (m/s)	N (rpm)	turbulence model	ρ(kg/m^3)	a_0 (m/s)	P_{ref} (Pa)
1	3	120	RSM	1025	1500	10^{-6}
2	5	250	RSM	1025	1500	10^{-6}

In table (2), N is rotational speed, Va is axial velocity of flow, ρ is density of water, a_0 is sound velocity and P_{ref} is reference pressure in underwater.

In this Numerical simulation six Hydrophones is used for extraction Sound Pressure Levels (SPLs). The Position of Hydrophones and their coordinates are shown in Figure 5 and Table 3, respectively. Typically in the case of a three-blade propeller operating at say 120rpm this gives a blade rate frequency of 6Hz and operating at say 250rpm this gives a blade rate frequency of 12.5Hz according equation(4), which is just below the human audible range of about 20 to 20 000 Hz [2].

$$f_m = mnf_r \tag{4}$$

Where:
m = harmonic number
n = number of blade
f_r = rotational frequency of the propeller

Table 3: Coordinates of Hydrophones.

Name	X-Coord.(m)	Y-Coord.(m)
Hydrophone 1	0.3	0.15
Hydrophone 2	0.5	0.2
Hydrophone 3	1.5	0.15
Hydrophone 4	0.3	0
Hydrophone 5	0.5	0
Hydrophone 6	1.5	0

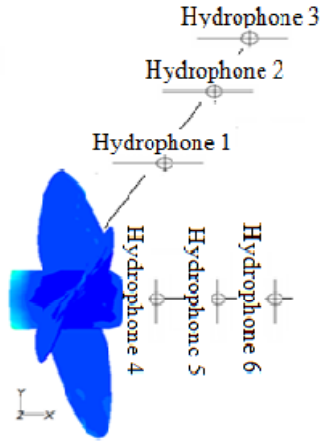

Figure 5: Position of Hydrophones for Numerical simulation.

3.0 RESULT AND DISCUSSION

3.1 Equations and Mathematical Expression

Noise prediction can be represented as the solution of the wave equation if the distribution of sources on the moving boundary (the blade surface) and in the flow field is known. FW-H formulated the following equation for the manifestation of acoustic analogy proposed by Light hill [9]:

$$\frac{1}{{a_0}^2}\frac{\partial^2 p'}{\partial t^2} - \nabla^2 p' = \frac{\partial^2}{x_i x_j}\left[T_{ij}H(f)\right] - \frac{\partial}{\partial x_i}\left(\left[P_{ij}n_j + \rho u_i(u_n - v_n)\right]\delta(f)\right) + \frac{\partial}{\partial t}\left([\rho_0 v_n + \rho(u_n - v_n)]\delta(f)\right) \tag{5}$$

$\acute{p}$ is the sound pressure at the far field ($\acute{p} = p - p_0$). $f=0$ denotes a mathematical surface introduced to "embed" the exterior flow problem (f>0) in an unbounded space, which facilitates the use of generalized function theory and the free-space Green function to obtain the solution. a_0 is the far-field sound speed, and T_{ij} is the Light hill stress tensor. The flow field is analyzed with finite volume method (FVM), and then the time-dependent flow field data are used as the input for FW-H formulation to predict the far-field acoustics.

3.2 Results for two different performance conditions

The cavitation number in each region of the blade was calculated using Equation (6) and (7). If the rotational speed of the propeller was low, the cavitation would be investigated at the root of the propeller *(r= 0)*, while the cavitation would be investigated at *r= 0.7R (R is the radius of blade (m))* [2] for higher speeds.

$$\sigma_{r=0} = \frac{P_0 - P_v}{0.5\rho V_a^2} \tag{6}$$

$$\sigma_{r=0.7R} = \frac{P_0 - P_v}{0.5\rho V_R^2} \tag{7}$$

V_a and $V_R = \sqrt{V_a^2 + (0.7Rw)^2}$ are velocities at $r= 0$ and $r= 0.7R$, respectively. w is the rotational speed of propeller *(rad/s)*. ρ is the water density *(kg/m^3)*. P_0 and P_v are the static pressure and water vapor pressure *(pa)*, respectively.

The contours of flow velocity and flow pressure are shown in Figures 6 and 7, respectively. According to maximum and minimum flow pressure, the cavitation number for first statue shown in Table 4. Sound Pressure level (SPL) for first and sixth Hydrophones are show in Figures 8 and 9, respectively.

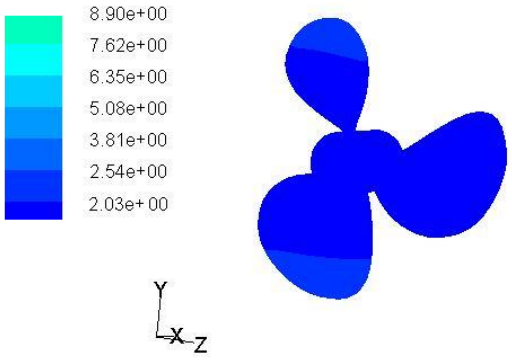

Figure 6: flow velocity contour [m/s] (V_a =3m/s , N=120rpm).

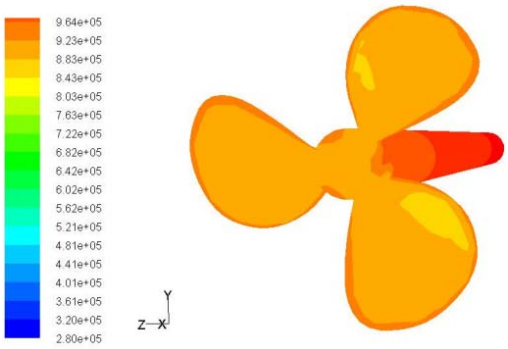

Figure 7: Flow pressure contour (pa) (V_a =3m/s, N=120rpm).

Table 4: Amount of cavitation number for first statue (for numerical and theory solve).

max and min σ for numerical simulation(v=3m/s , w=120rpm)	
max and min σ by theory formulation(v=3m/s , w=120rpm)	
error(v=3m/s , w=120rpm)	
max and min σ for numerical simulation(v=5m/s , w=250rpm)	

Flow solve for second statue show that cavitation number is too lower than first statue. The Contours of flow velocity and flow pressure are shown in Figures 10 and 11, respectively. According to maximum and minimum pressure of flow amount of cavitation number for second statue, is shown in Table 4. The SPL for first and sixth Hydrophones are show in Figures 12 and 13, respectively.

What can be harvested from figures 8, 9, 12 and13 amount of the SPL in second statue is more than first statue. In second statue with increase of flow velocity and rotational speed, flow on blade surface is closed to inception sheet of cavitation. Increase in distance of propeller results increase sound pressure levels (SPLs) which is observed clearly in figures 8 and 9 or 12 and 13.

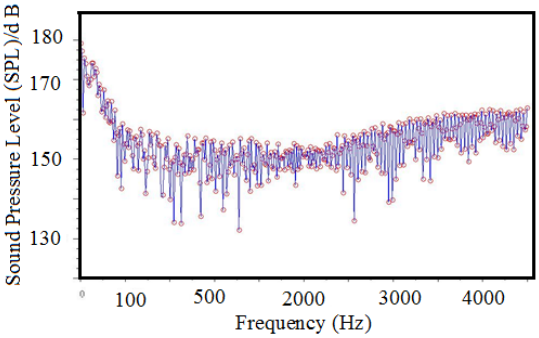

Figure 8: Sound pressure level for hydrophone 1 (V_a =3m/s, N=120rpm).

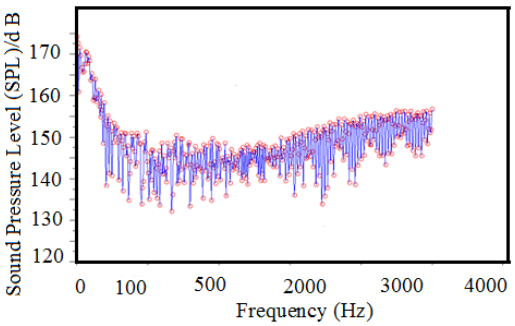

Figure 9: Sound pressure level for hydrophone 6 (V_a =3m/s, N=120rpm).

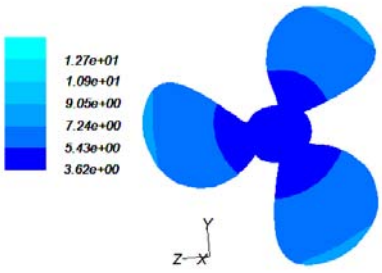

Figure 10: Flow velocity contour (m/s) (V_a =5m/s, N=250rpm).

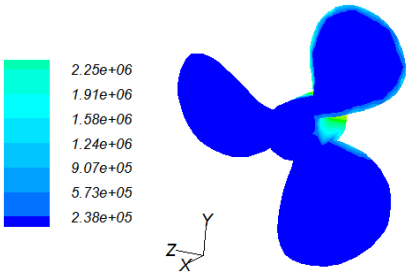

Figure 11: Flow pressure contour (pa) (V_a =5m/s, N=250rpm).

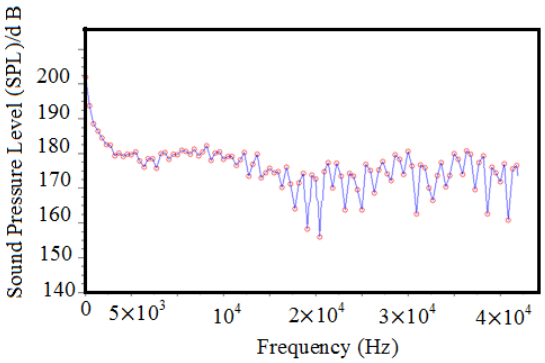

Figure 12: Sound pressure level for hydrophone1 (V_a=5m/s, N=250rpm).

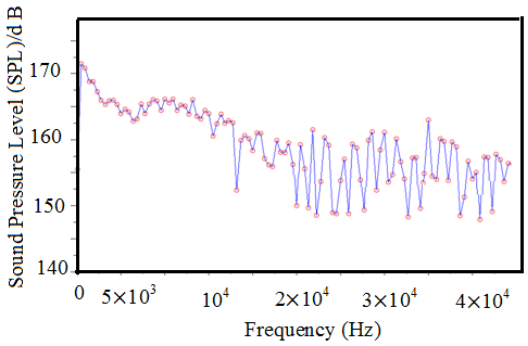

Figure 13: Sound pressure level for hydrophone 6 (V_a =5m/s, N=250rpm)

5.0 CONCLUSION

In this paper, different operating conditions of a propeller model was studied in order to find the ranges of the cavitation initiation and its development and to study the effect of cavitation on the SPLs.

The non-cavitating and blade sheet cavitation noise generated by an underwater propeller is analyzed numerically in this study. The flow field is analyzed with finite volume method (FVM), and then the time-dependent flow field data are used as the input for Ffowcs Williams–Hawkings formulation to predict the far-field acoustics. Noise characteristics are presented according to noise sources and conditions. According to results cavitation going to incept by increase of flow velocity and propeller revolution speed.

In present working two statue velocity and revolution speed was performed which second the statue closed to inception cavitation without cavitiation occurrence so calculated noise in this paper is due to dipole and quaderpole source in light hill equation. With inception cavitation, dominate source of noise is monopole noise which is due to initiation and development of cavitation.

Numerical analysis based on theory provides a basis for cavitation study and scaling of experimentally measured data.

Since hydrophone 1 is located near sound source, the overall SPL for hydrophone 1 is more than hydrophone 6. When the pressure decreases, the cavitation initiation develops. As can be seen from results ranges of SPLs increase with increasing rotational speed of propeller.

The results showed that in the process of initiation of cavitation formation, the increasing effect of rotational speed of propeller was stronger than flow velocity.

The obtained results can be used to optimize the experimental parameters of derivated patterns of noise radiation.

REFERENCE

1. Ross, D. (1976). Mechanics of Underwater Noise Pergamon Press.
2. Carlton, JS. (1994). Marine Propellers and Propulsion, *Butterworth Heinemann, London.*
3. Seol, H., Jung, B., Suh, JC., Lee, S. (2005). Development of hybrid method for the prediction of underwater propeller noise, *J Sound and Vibration 228: 345-360.*
4. Sharma, S.D., Mani. K., Arakeri V.H. (1990). Cavitation Noise Studies on marine propellers, *J Sound and Vibration 138(2): 255-283.*
5. Jin-ming, Y., Ying, X., Fang, L., zhan-zhi, W. (2012). Numerical prediction of blade frequency noise of cavitating propeller, *J Hydrodynamics* 24(3): 371-377.
6. Bagheri, M.R., Seif, M.S., Mahdigholi, H. (2013) Hydrodynamic and acoustic analysis of underwater propellers by numerical method (in Iran), *International Journal of Maritime Technology.*
7. Bagheri, M.R., Seif M.S., Mahdigholi, H. (2012). Numerical Simulation of underwater propeller noise (in Malaysia), *Proceeding of 12th International Conference on Marine Technology, Kuala Terengganu, Malaysia.*
8. Bagheri, M.R., Seif, M.S., Mahdigholi, H. (2012). Numerical simulation of underwater propeller non-cavitating noise by FVM method (in Iran), *Proceeding of 2nd International conference on Vibration and Acoustic*, Iran, Sharif University of Technology.
9. Light hill, MJ. (1952). on sound generated aerodynamically. I. General theory, *Proc, R. Soc. Lond,* vol. 211 no. 1107 564-587.
10. Arazgaldi, R., A. Hajilouy, B. Farhanieh (2009). Experimental and Numerical Investigation of Marine Propeller Cavitation. Sharif University of Technology, *Journal SCIENTIA IRANICA,* Vol. 16, No. 6, pp. 525-533.
11. Ffowcs Williams, JE., Hawkings ,DL. (1969). Sound generated by turbulence and surfaces in arbitrary motion, *Philosophical Transactions of the Royal Society A 264 (1151) 321–342.*
12. Singhal, A.K., Athavale, M.M., Li H., Jiang, Y .(2002). Mathematical basis and validation of the full cavitation model, *ASME J. Fluids Eng, pp. 617-624.*